NONLINEAR FRACTURE MECHANICS-BASED ANALYSIS OF THIN WALL CYLINDERS

Frederick W. Brust
Brian N. Leis
Thomas P. Forte
Battelle Memorial Institute
Columbus, Ohio

SUMMARY

This paper presents a simple analysis technique to predict the crack initiation, growth, and rupture of large-radius, R, to thickness, t, ratio (thin wall) cylinders. The method is formulated to deal both with stable tearing as well as fatigue mechanisms in applications to both surface and through-wall axial cracks, including interacting surface cracks. The method can also account for time-dependent effects. Validation of the model is provided by comparisons of predictions to more than forty full scale experiments of thin wall cylinders pressurized to failure.

INTRODUCTION

This paper summarizes the results of a series of papers (refs. 1-9) which describe the development, application, and verification of a simple methodology to predict failure in large R/t cylinders (greater than 40). While the methodology was developed for the natural gas pipeline industry, where failures can lead to serious consequences, it should be equally applicable to the airline industry since the toughness of line pipe steel and aircraft aluminum are quite similar. The methods are applicable for both through-wall and surface cracks, although the main focus here is on the surface cracks. The general methodology has been developed for time-dependent primary creep crack growth, with the special case of the elastic-plastic crack growth incorporated. The method has been programmed into a user friendly personal computer-based code (ref. 10), which is currently being used by non-experts to devise line pipe hydro-proof test strategies to certify line pipe.

The paper first discusses the importance of time-dependent effects, first on gas line pipe steel and then for aluminum, at and below room temperature. The predictive model is described next, as developed to predict fracture for surface cracked cylinders. The method is based on classical J-Tearing theory, with J estimated via a plastic zone correction technique for the surface crack problem. Next, two examples are discussed, one which deals with a through-wall crack in a pipe which experiences time-dependent crack growth, and then a summary of more than forty predictions compared to experimental data. Finally, a discussion of multiple interacting surface cracks and the extension of the model to multiple interacting cracks is considered.

IMPORTANCE OF TIME DEPENDENCE

Because of its usual association with thermally activated creep, time-dependent deformation and its corresponding effect on the crack growth and failure process are often considered to be important only at high temperatures. However, an increasing body of experimental evidence suggests that, for many materials, time-dependent effects cannot be neglected for quasi-static loading rates even at room temperature or below. Primary creep will occur in these situations if the stress is sufficiently high. Obviously, near a crack tip the stresses are very high, so that near a crack tip time dependent deformation may be manifest in the form of primary creep. Time- dependent deformation near a crack tip may lead to creep crack growth in addition to the time-independent (plastic) crack growth which is usually considered.

Since prediction of failure loads is usually performed by neglecting time- dependent deformation (at lower temperatures), non-conservative predictions may often result. This is particularly true for structures which are routinely subjected to proof tests such as gas pipelines, or certain aerospace structures. Indeed, proof tests are performed to ensure service reliability for a structural component by assuming that cracks which may lead to catastrophic failure in service will be removed during the test. Parts which fail during the proof test are then replaced, thus presumably avoiding catastrophic service failures.

Unfortunately, for ductile materials, proof tests may cause a crack to grow without failing the component. In fact, the crack may grow to a length which will lead to component failure during service at relatively moderate loads due to the history-dependent damage which occurs at the crack tip during the proof test. Time- dependent crack growth greatly enhances this effect. Hence, it is very important to be able to quantify the effects of time-dependent, as well as time-independent, crack growth and damage which occur during a proof test and, correspondingly, the effect of this damage on the subsequent service loading must be understood.

A somewhat detailed summary of time-dependent deformation of steels has been provided in refs. 4, 6-9 and, as such, will not be repeated here. However, because this behavior is not unique to steels and has been observed for some time in aluminum and other materials used in aerospace applications, a brief discussion of some of the earliest data to document the time dependent behavior of aluminum at and below room temperature (ref. 11) follows here before the model to deal with coupled creep and plasticity is presented. Tiffany and Masters in 1964 presented some of the earliest data that indicate the relative effects of high stress induced creep and its effect on crack growth, specifically for surface-flawed 2219-T87 aluminum specimens tested in liquid nitrogen. Those results showed that as the stress intensity increased above some threshold level, sustained loading below K_{Ic} caused failures at times that decreased from the order of hundreds of hours to near zero as the critical value of the stress intensity was approached. For that specific material, the threshold for sustained load cracking at liquid nitrogen temperatures was about 0.9 K_{Ic}. Similar trends have been developed since for a variety of materials and applications. It follows that care must be taken to ensure that such growth does not confound attempts to ensure integrity through proof testing and to avoid failures due to this mechanism. It is to this end that the following model was developed.

ANALYSIS MODEL - SURFACE CRACKS

The general model for predicting cylinder failure in the presence of surface cracks is presented here. The general theory for predicting elastic-plastic and primary creep crack growth is provided in ref. 4. The extension of the model to handle through-wall axial cracked cylinders is provided in refs. 7-8, and details of the surface crack model are provided in refs. 6 and 9. Here we provide only the final equations for the axial surface cracked cylinder to illustrate the simplicity of, and ease of use for, the model.

Because elastic-plastic estimation schemes are not available for evaluating J for surface cracks in cylinders except for special cases, the model is based on an adaptation of elastic solutions for J. For elliptic surface cracks subjected to tensile loading, detailed compilations of finite element solutions are readily available in the literature if linear elastic conditions prevail. The primary creep model consists of estimating J by using a time-dependent Irwin estimate of the plastic zone in the elastic solution. Referring to fig. 1 for geometric definitions of the pipe and flaw, the elastic component, J_e, is written as:

$$J_e = \sigma^2\left(\frac{\pi a}{Q}\right) \left\{F(c/a,\ a/t,\ R/t,\ \phi)\right\}^2 \left\{E/(1 - \upsilon^2)\right\}^{-1} , \qquad (1)$$

where σ is the applied stress due to the pressure, P, (σ, = PR/t), Q is the square of the complete elliptic integral of the second kind, and ϕ defines the location along the crack front where J_e is evaluated (see fig. 1). In addition, R, t, c, and a are defined in fig. 1, and E and ν are the elastic modulus and Poisson's ratio, respectively. The F-function in Equation (1) has been compiled in ref. 12 for R/t = 40 using the Atluri (ref. 13) SNA version of the finite element alternating method. For present purposes, the value of Q is taken in the form of the Newman and Raju approximation (ref. 14), i.e.,

$$Q = 1 + 1.464\ (a/c)^{1.65} , \quad a/c \le 1.0$$
$$Q = 1 + 1.464\ (c/a)^{1.65} , \quad a/c \ge 1.0 . \qquad (2)$$

Plastic and Primary Creep Component of $J_p(t)$

The time-dependent nonlinear component of J for external axial surface cracked pipes is estimated by including a nonlinear correction to the elastic solution based on the inelastic time-dependent field at the flaw. Resorting to this approximation derives from the fact that the time-dependent component of J could not be interpolated from any known finite element solutions, since no compilation or general

numerical solutions are available for surface cracked pipes with formal consideration of inelastic effects.

The concept of a time-dependent plastic zone at the crack tip is natural given that primary creep rather than secondary creep is considered to occur during the short-time higher pressure excursions during hydrotesting. During the initial loading, a plastic zone develops whose size varies along the length of the flaw. During the hold periods, primary creep develops apparently due to the high stress which occurs at the crack tip all along the crack front. Because the time-independent hardening exponent is greater than the creep exponent, "loading" occurs at the crack tip along the crack front during the hold period (see ref. 4). Hence, during hold periods the crack tip inelastic zone grows along the crack's length. The nonlinear component of J is time dependent since, as the plastic zone grows in size during the hold periods, J increases.

Theoretical considerations indicate that good estimates of J can only be assured if the inelastic zone remains relatively small when using this method of estimating J. Despite this limitation, the method will be applied in cases where the plastic zone is large compared to the crack depth, as occurs, for example, for deep cracks near failure load. In such limiting cases, the calculated size of the inelastic zone may be larger than the remaining uncracked ligament in front of the crack tip at the deepest point along the crack front. This is physically unrealistic, so that, under these circumstances, the use of a plastic zone-type correction to the elastic solution to estimate J is viewed as a compliance correction technique.

The size of the plastic zone ahead of the crack tip has been estimated by analogy to the approach suggested by Kujawski and Ellyin (ref. 15): viz,

$$r_p = \frac{2\,\hat{n}}{\hat{n}+1}\left[\frac{K^2}{\beta\pi s_y^{\,2}}\right] \tag{3}$$

$\beta = 2$ Plane σ (at tips, $\phi = 90°$ fig. 1)
$\beta = 6$ Plane ϵ (at tips, $\phi = 0°$ fig. 1).

The value of $\hat{n}$ in Equation (3) is calculated as:

$$\hat{n} = \frac{W_y^e + W_y^p}{W_y^e + W_y^p/n} \tag{4}$$

with the partitioned energy densities defined as:

$$W_y^e \equiv \frac{s_y^{\,2}}{2E} \quad , \tag{5a}$$

and

$$W_y^p \equiv \left[\frac{n}{n+1}\right] s_y \epsilon_y^p \quad . \tag{5b}$$

In Equation (5), s_y is the yield stress and ϵ_y^p is the amount of plastic strain at yield, which is often defined as the 0.2 percent offset strain. For a Ramberg-Osgood stress-strain law :

$$\frac{\epsilon}{\epsilon_o} = \frac{\sigma}{\sigma_o} + \alpha\left[\frac{\sigma}{\sigma_o}\right]^n \quad . \tag{6}$$

The value of ϵ_y^p is given by:

$$\epsilon_y^p = (\alpha\epsilon_o)\left[\frac{\sigma_y}{\sigma_o}\right]^n \quad , \tag{7}$$

where, as detailed earlier, α and n are correlated through σ_o, and are history dependent.

It follows that the nonlinear component of J, $J_p(t)$ is given by:

$$J_p(t) = (\sigma)^2 \left\{\frac{\pi(r_p(t))}{QE/(1-\nu^2)}\right\} \{F^2(a/t,\ c/a,\ \phi)\} \quad , \tag{8}$$

where $r_p(t) = r_p(n(t),\ \alpha(t))$. The value of J is then found as the sum of Equations (1) and (8).

The Material Resistance Curve. In a series of tests on compact tension specimens, Kuhnle and Riedel (ref. 16) have shown that the J-resistance curves are independent of load-hold effects for thermal conditions between room temperature and 300 F. The specimens were each subjected to various types of loading conditions, such as varying load-hold times, varying displacement rates, constant load, and in all cases the J-resistance curves are very similar. However, there is a temperature dependence, with the J-R curves lowering as temperature increases. Our results (see refs. 4-9) have also shown the same trend as observed in ref. 16.

This means that once a J-resistance curve is developed at a given temperature, it may be used to predict the crack growth behavior of cracked bodies experiencing creep deformation, provided that the creep is mainly primary. For our model, the J-resistance curves were developed using standard elastic-plastic loading rates and conditions and are assumed to be valid for analysis during creep conditions. This is important since it allows only one resistance curve to be developed and this curve is independent of loading rate. This, of course, assumes that dynamic loading of the specimens does not occur; i.e., the loading is typical for quasi-static conditions.

MODEL PREDICTIONS AND COMPARISONS WITH EXPERIMENTAL DATA

This section provides two example comparisons of model predictions to experimental data. The first example illustrates the predictive ability of the model for a case where time-dependent behavior is important for an axially through-wall cracked cylinder. The second example shows a comparison of model predictions compared to experimental results for more than 40 full-scale pipe experiments where time dependence was not important.

Axial Through-Wall Cracked Cylinder

A 22-inch outer diameter by 0.27-inch-thick pipe made of X52 line pipe steel was subjected to the pressure-time history shown in fig. 2. As seen here, the pipe was subjected to a series of load-hold sequences until failure occurred at 1100 psi. Initially, it took some time (about 100 minutes) to load the pipe to the first hold pressure of 775 psi. However, after the initial load was applied, subsequent load times required between 45 and 120 seconds, and these appear as vertical lines (step functions) in fig. 2. The analysis model assumes that the load periods occur instantaneously, and then the hold period begins. The implications of this assumption in terms of predicted failure pressure and crack growth versus time predictions are small. However, for history-dependent loading situations, the time it takes to load the specimen may be important. A discussion of the implications of history-dependent loading on the primary creep model is provided in ref. 8.

The estimation scheme for an axial through-wall cylinder is somewhat different from that summarized above for a surface-cracked cylinder and is provided in refs. 4 and 7. The material properties, both time-dependent tensile properties and the J-Resistance curve, are listed in ref. 7 and are not provided here so that the results may be emphasized.

For the pressure-time history imposed to the pipe shown in fig. 2, the predicted pressure versus crack growth history is illustrated in fig. 3. Also shown in fig. 3 are plots of the experimental pressure versus crack growth history. Note that the experimental results for both crack tips are shown here since symmetric crack growth did not occur at both crack tips in the experiment. Good prediction of the experimental behavior is evident. Also plotted in fig. 3 is the predicted behavior neglecting time-dependent damage accumulation. It is clear that neglecting the primary creep behavior which occurs in the highly stressed crack tip region can result in non-conservative prediction of failure pressure. Neglecting time-dependent damage mechanisms in the flaw growth process overpredicts the failure pressure by about ten percent here. This has serious implications with regard to proof-test methodology.

The predicted crack length versus time behavior is compared to the experimental data for both crack tips in fig. 4. Very good comparison is observed up to about 25,000 seconds. Reasonable predictions are also observed beyond this point although slightly shifted in time. Near failure, and at failure, where the amount of crack growth precludes valid J-Tearing theory, it is seen that predicted crack growth underestimates the experimental data. This underprediction of crack growth is also observed for time-independent analyses based upon J-theory (see, for instance, ref. 17). However, the predicted failure pressure compares quite well with experimental results. Predictions are compared to experiments for several other crack sizes and cylinder dimensions and loading conditions, as discussed in refs. 7 and 18.

Axial Surface-Cracked Cylinder Analysis

The experimental database in ref. 19 is considered tentatively to represent an average pool of data, and predictions are based on the average fracture trends. The J-Resistance curves for the test data in ref. 19 are not available since, at the time of these tests, other fracture parameters were used to characterize fracture. As such, average J-resistance behavior was characterized in terms of flow stress and CVP (Charpy) full-size energy, which were routinely determined for these materials at the time of these tests. The equation used to convert these parameters to a usable J-Resistance curve was developed in ref. 20. The time-dependent Ramberg-Osgood relations were developed from isochronous stress-strain tests, as discussed in refs. 6-9. The analyses are performed free of "selective calibration" that might be used (inappropriately) on a case-by-case basis to enhance the quality of the predictions, i.e., only one set of material data were used for all cases about to be discussed.

Values of predicted and observed failure pressure are shown in fig. 5 for comparison and evaluation of the analysis method. Figure 5a directly compares failure pressures with the predicted result on the ordinate, P_p, and the observed experimental result on the abscissa, P_e. This figure does not show any particular bias as a function of observed pressure nor is there a particular bias in regard to steel grade or processing history. The mean slope is 1.0415, with a standard deviation of 0.0977. This means that, on average, the model predictions are slightly conservative, which, in turn, means that the average J-resistance behavior is slightly overpredicted by the average trends representing the relationship between flow stress and Charpy data, as developed in ref. 20. Fig. 5b shows that there is no bias in the predictions as a function of a/t. That is, the ratio of predicted to observed failure pressure scatters evenly for all values of the abscissa, a/t. Likewise, this figure shows no particular bias as a function of c/a. Finally, fig. 5c shows these results reasonably fit a normal distribution consistent with the assumption that this pooled experimental database represents an average collection of observed failure pressures. Note that the J-tearing theory (Equations 1 to 8) was found to control all but one of the predictions in this dataset. Only the test for a/t = 0.92 was controlled by the net-section criterion.

The analysis of these test results has assumed that all flaw growth in these tests is time-independent. The pressure increased in these tests at about 20 psig-minute (ref. 19), so that some creep-tearing is possible as the pressure approaches the failure pressure. This time-dependent growth can only occur at or above pressures causing $J \sim J_{Ic}$. Analysis of a series of typical flaw depths and lengths indicated this occurred over the last 5 to 10 percent of the pressurizing. Calculations with time dependence during this interval showed little difference in the predicted failure pressure, as compared to the behavior predicted assuming elastic-plastic conditions only. Accordingly, the difference between the predicted and observed results is, on-average, not due to the idealization of neglecting time dependent effects. The difference is therefore ascribed to the definition of "average" fracture properties in ref. 18, using that rather limited database for pipe steels to represent the average behavior for this larger dataset.

INTERACTING SURFACE CRACKS

Because many practical failure situations involve multiple cracks, with failure being a consequence of the interaction and coalescence of such cracks, the present model for primary creep is currently being extended to address this class of problem. To date, analyses have been completed exploring this problem idealized in terms of a pair of cracks (ref. 21). This work has explored this problem through a range of analyses that again have been made using the finite-element alternating method (FEAM). The numerical procedure as adapted to this class of problem is detailed elsewhere (refs. 12 and 21), while ref. 21 provides some of the available results.

Fig. 6 provides an overview of the crack-pairs geometry discussed in ref. 21. With regard to fig. 6, note that the geometry addressed represents a surface-cracked flat-plate which, as detailed in ref. 12, can be used to represent the cracking behavior in cylinders with diameter-to-wall thickness ratios that are greater than about 40, so that the related results encompass many aerospace situations. Analysis has been done for cases where the axial and circumferential spacing between the tips of a pair of geometrically identical cracks have been systematically varied for a limited set of crack length-to-depth ratios. These analyses were done to determine the relative spacings between tips for (1) positive interaction (i.e., K increases) or shielding (i.e., K decreases) and (2) to assess conditions for coalescence. The length-to-depth ratios studied were selected to represent typical stress-corrosion cracking (SCC) geometries, which was the motivation for much of this work (ref. 22). This consideration led to flaw length-to-depth ratios (i.e., 2c/a) in the range of $1 \leq 2c/a \leq 6$. With reference to fig. 6, the analysis for crack-pairs has been done to represent axial tip spacings in the range $-3 \leq 2d/t \leq 1$ for circumferential tip spacings in the range $0 \leq 2b/t \leq 1$.

Figs. 7a through 7c show typical results for Mode I, II, and III cracking, respectively. These mixed-mode results are used here to illustrate the role of Modes II and III as drivers for trends observed in SCC coalescence. Results in fig. 7 represent $a/t = 0.5$ (i.e., depth = half the wall thickness) and $c/a = 3$ (i.e., length = 6 times the depth), for $2d/t = -3$, which in this case defines co-parallel cracks (i.e., cracks stacked above each other). With reference to fig. 6, $\phi = 0$ represents the intersection of the crack with the surface while $\phi = 90$ is the location of maximum depth. Decreasing values of 2b/t denote a decreasing circumferential spacing while increasing values of 2d/t indicate increasing axial spacing.

Note by comparing the results for Modes II and III with the Mode I trends that K_{II} is about 0.1 K_I, whereas K_{III} is still smaller and shows a sign change around the crack front. The nature of the shear modes is to cause the tips of vertically stacked (co-parallel) cracks to grow toward each other for the portions of these cracks near the surface. Analysis similar to that shown in fig. 7 for other flaw spacings indicates the tendency for nearly co-linear cracks to hook toward the other crack. As with the case of the co-parallel (stacked) cracks, the shear components (Modes II and III) drive this process. Both features are observed in patches of SCC. Such features also occur for mutually adjacent crack tips for fatigue crack growth, which indicates that the mechanics of the process rather than the mechanism controls such features. It follows that fracture mechanics should provide a viable basis to characterize coalescence and failure for SCC.

Results similar to those shown in fig. 7 for Modes I, II, and III across a range of other lateral spacings continue to be developed to assist in formulating criteria for coalescence and failure in

situations where the local and global compliance are altered by the presence of multiple surface cracks. These studies currently include idealized arrays of cracks as well as specific configurations typical of failures in thin-walled cylinders (ref. 23).

SUMMARY and CONCLUSIONS

This paper has presented and discussed an engineering analysis technique to predict the crack initiation, growth, and rupture of large-radius, R, to thickness, t, ratio (thin wall) cylinders. The method was discussed in terms of stable tearing although it has been formulated to also deal with fatigue mechanisms in applications to both surface and through-wall axial cracks, including interacting surface cracks. The method was formulated and discussed with reference to the analysis of time-independent as well as time-dependent effects. Validation of the model was discussed in terms of comparisons of predictions to the actual failure behavior of more than forty full-scale experiments of thin-wall cylinders pressurized to failure. Validation beyond that discussed herein indicates the suitability of this same engineering concept for fatigue loadings in thin-walled cylinders as well as for more complex loading histories. Finally, the extension of this concept to serve as a failure criterion in applications involving multiple cracks was discussed.

The primary conclusion of this work is that an engineering model has been developed that provides reasonably accurate solutions for the stability and growth of cracks in thin-walled cylinders. While the majority of the applications of this model have been to steel structures, the underlying concepts can be extended to most engineering materials in otherwise comparable situations.

REFERENCES

1. Leis, B. N.; and Brust, F. W.: Hydrotesting Effects - 1. *Oil and Gas Journal*, February 12, 1990, pp. 45-48.

2. Leis, B. N.; and Brust, F. W.: Hydrotesting Effects - Conclusion. *Oil and Gas Journal*, February 19, 1990, pp. 52-54.

3. Brust, F. W.; and Leis, B. N.: A Study of Primary Creep Crack Growth at Room Temperatures. *Numerical Methods in Fracture Mechanics*, Editors Luxmoore & Owen, Proceedings of the 5th ICNMFM, Freiburg, West Germany, April, 1990.

4. Brust, F. W.; and Leis, B. N.: A New Model for Characterizing Primary Creep Damage. *Int. Journal of Fracture*, vol. 54, pp. 45-63, 1992.

5. Brust, F. W.; and Leis, B. N.: The Effects of Primary Creep on Elastic-Plastic Crack Growth. *Fatigue, Degradation, and Fracture, 1990*, ASME Special Publication, vol. 195, June, 1990.

6. Brust, F. W.; and Leis, B. N.: Primary Creep Crack Growth at Room Temperature in Surface Cracked Pipes. *Int. Journal of Pressure Vessels and Piping*, vol. 52, pp. 273-298, 1992.

7. Brust, F. W.; and Leis, B. N.: A Model for Predicting Primary Creep Damage in Axial Cracked Cylinders, Part I, Theory. *Engineering Fracture Mechanics*, vol. 4, pp. 615-627, 1992.

8. Brust, F. W.; and Leis, B. N.: A Model for Predicting Primary Creep Damage in Axial Crack Cylinders, Part II, Applications, *Engineering Fracture Mechanics*, vol. 43, no. 4, pp. 629-639, 1992.

9. Leis, B. N.; and Brust, F. W.: Validation of Room-Temperature Primary Creep Crack-Growth Analysis For Surface Cracked Pipes, *Nuclear Engineering and Design*, vol. 142, pp. 69-75, 1993.

10. Leis, B. N.; and Ghadiali, N.D.: *Pipe Axial Flaw Failure Criteria -- PAFFC Version 1.0 User's Manual and Software*. American Gas Association, NG-18 Report No. 211, April 26, 1994.

11. Tiffany, C. F.; and Masters, J. N.: *Applied Fracture Mechanics*. ASTM STP 381, pp. 249-278, 1964.

12. Stonesifer, R. B.; Brust, F. W.; and Leis, B. N.: Stress-Intensity Factors for Long Axial Outer Surface Cracks in Large R/t Pipes. *Fracture Mechanics: Twenty-Second Symposium*, Vol. II, ASTM STP 1131, 1992, pp. 29-45.

13. Nishioka, T.; and Atluri, S. N.: Analytical Solution for Embedded Elliptical Cracks, and Finite Element Alternating Method for Elliptical Surface Cracks Subjected to Arbitrary Loadings. *Engineering Fracture Mechanics*, vol. 17, no. 3, pp. 247-268, 1983.

14. Newman, J. C.; and Raju, I. S.: An Empirical Stress-Intensity Factor Equation for the Surface Cracks. *Engineering Fracture Mechanics*, vol. 15, no.1-2, pp. 185-192, 1981.

15. Kijawski, D.; and Ellyin, F.: On the Size of Plastic Zone Ahead of Crack Tip. *Engineering Fracture Mechanics*, vol. 25, no. 2, pp., 229-236.

16. Kuhnle, V.; and Riedel, H.: Time-Dependent Deformation and Fracture of Steel Between 20 and 400 C. *International Journal of Fracture*, vol. 34, pp. 179-194, 1987.

17. Hutchinson, J. W.; and Paris, P. C.: *Stability of Analysis of J Controlled Crack Growth.* ASTM STP 668, pp. 37-64, 1979.

18. Leis, B. N.; Brust, F. W.; and Scott, P. M.: *Development and Validation of a Ductile Flaw Growth Analysis for Gas Transmission Line Pipe*. American Gas Association, Cat. No. L51543, June 1991.

19. Kiefner, J. F.; Maxey, W. A.; Eiber, R. J.; and Duffy, A. R.: *Failure Stress Levels of Flaws in Pressurized Cylinders*. ASTM STP 536, pp. 461-481, 1973.

20. Leis, B. N.; and Brust, F. W.: *Ductile Fracture Properties of Selected Line Pipe Steels*. American Gas Association, Catalog No. L51604, January 1990.

21. Stonesifer, R. B.; Brust, F. W.; and Leis, B. N.: Mixed Mode Stress Intensity Factors For Interacting Semi-Elliptical Surface Cracks In A Plate. *Engineering Fracture Mechanics*, vol. 45, no. 3, pp. 357-380, 1993.

22. Leis, B. N.; and Parkins, R. N.: Modelling Stress-Corrosion Cracking of High-Pressure Gas Pipelines. Paper 19 in Eighth Symposium on Line Pipe Research proceedings, American Gas Association, Catalog No. L51680, September, 1993.

23. Leis, B. N.; and Mohan, R.: Failure Criteria for Pipeline Flaws. Paper 9 in Eighth Symposium on Line Pipe Research proceedings, American Gas Association, Catalog No. L51680, September, 1993.

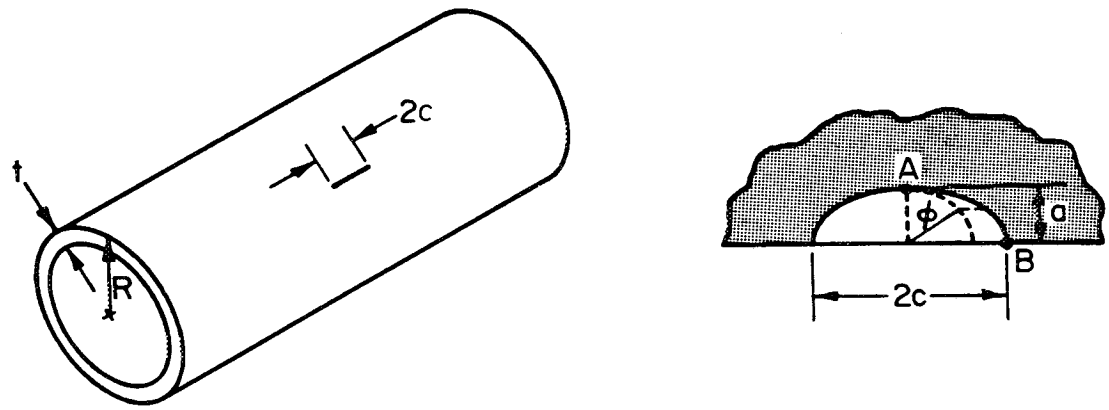

Figure 1. Geometric parameters for part-through-wall flawed cylinders.

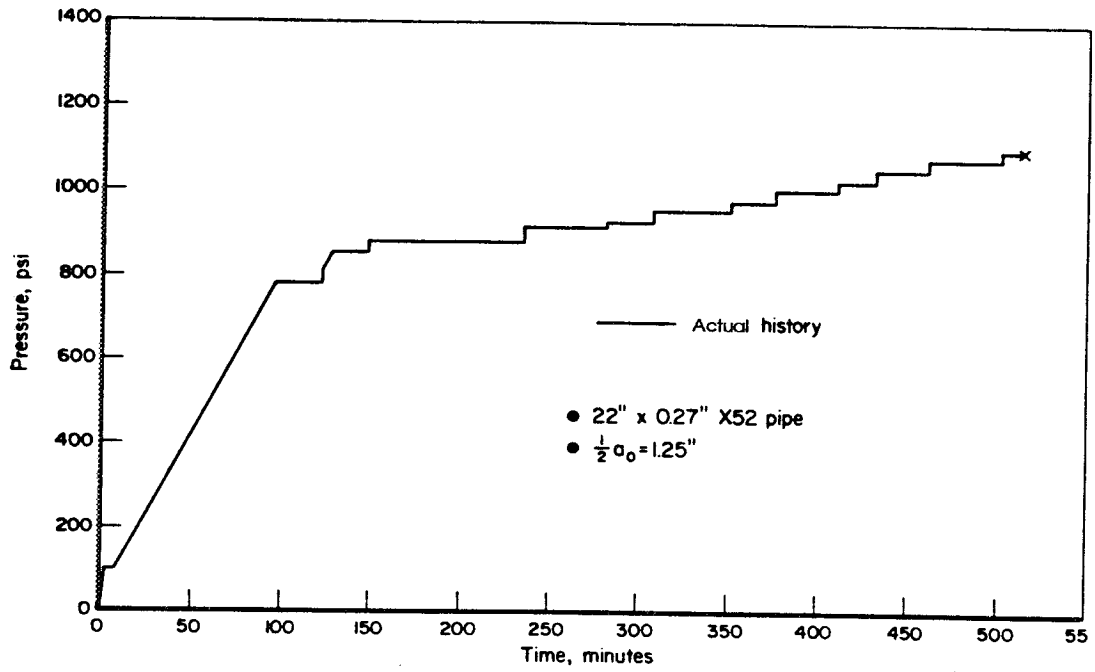

Figure 2. Pressure versus time history applied to 22-inch through-wall cracked pipe.

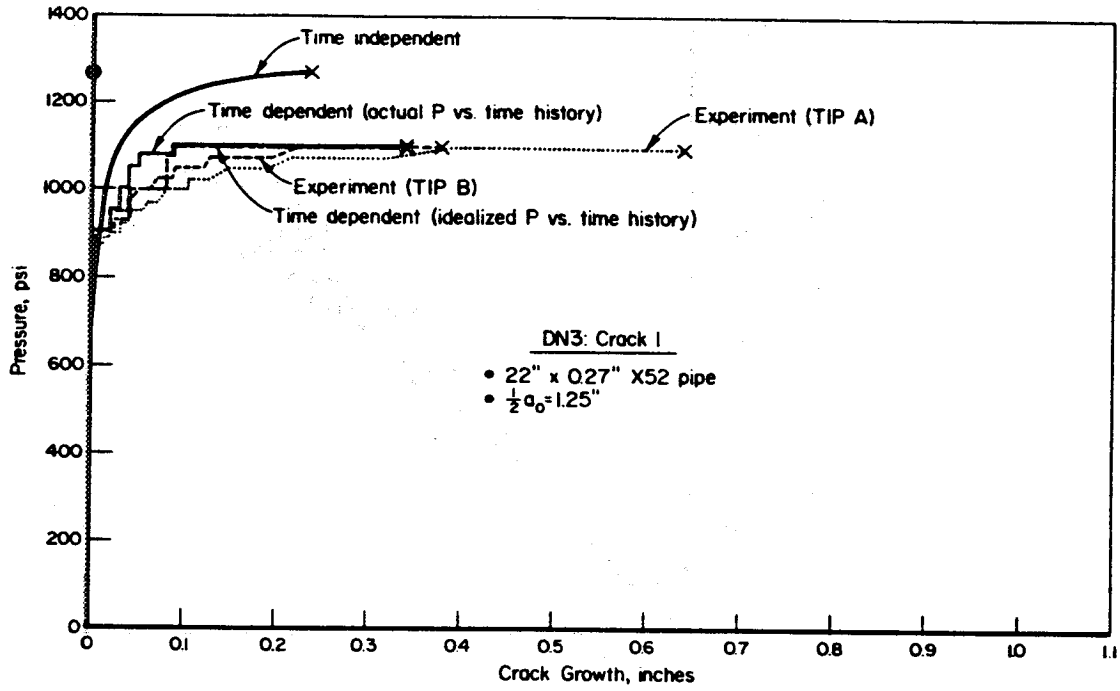

Figure 3. Results for full-scale test DN3.

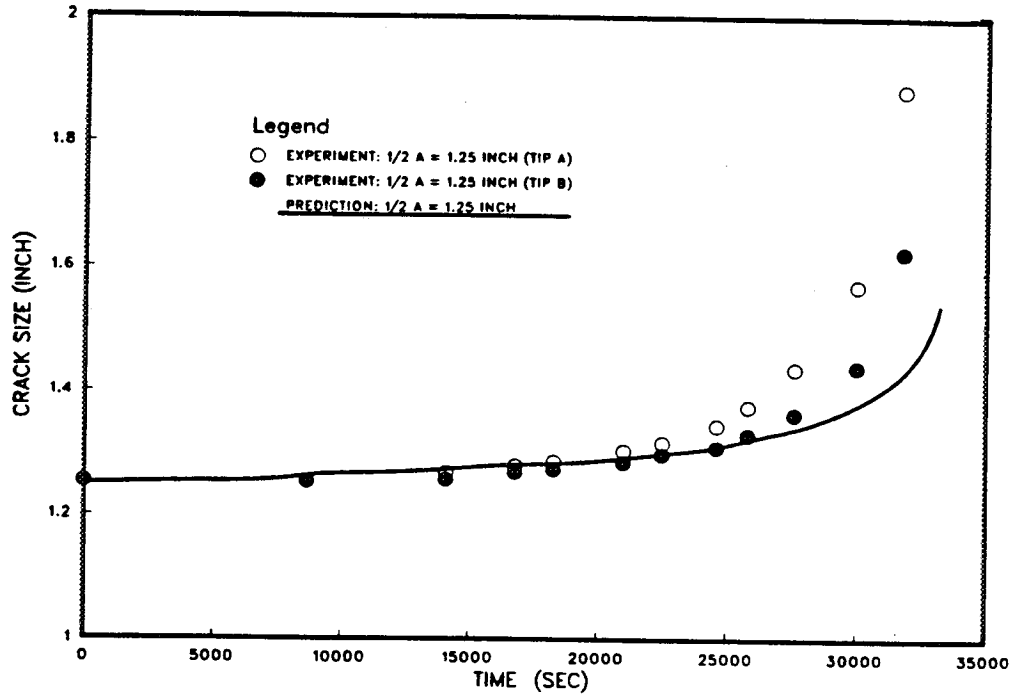

Figure 4. Crack size versus time for 22-inch pipe.

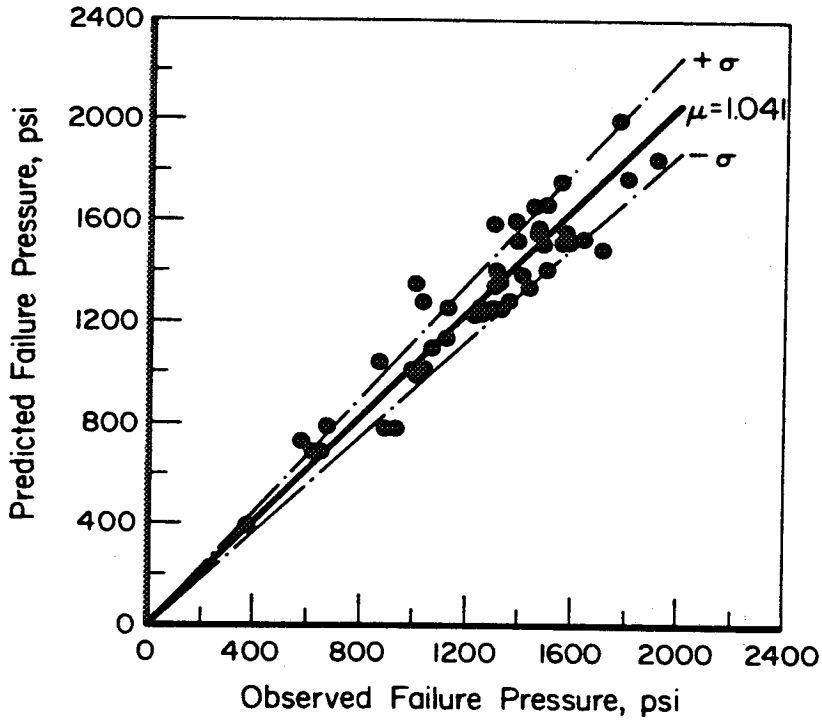

(a) P_p versus P_e

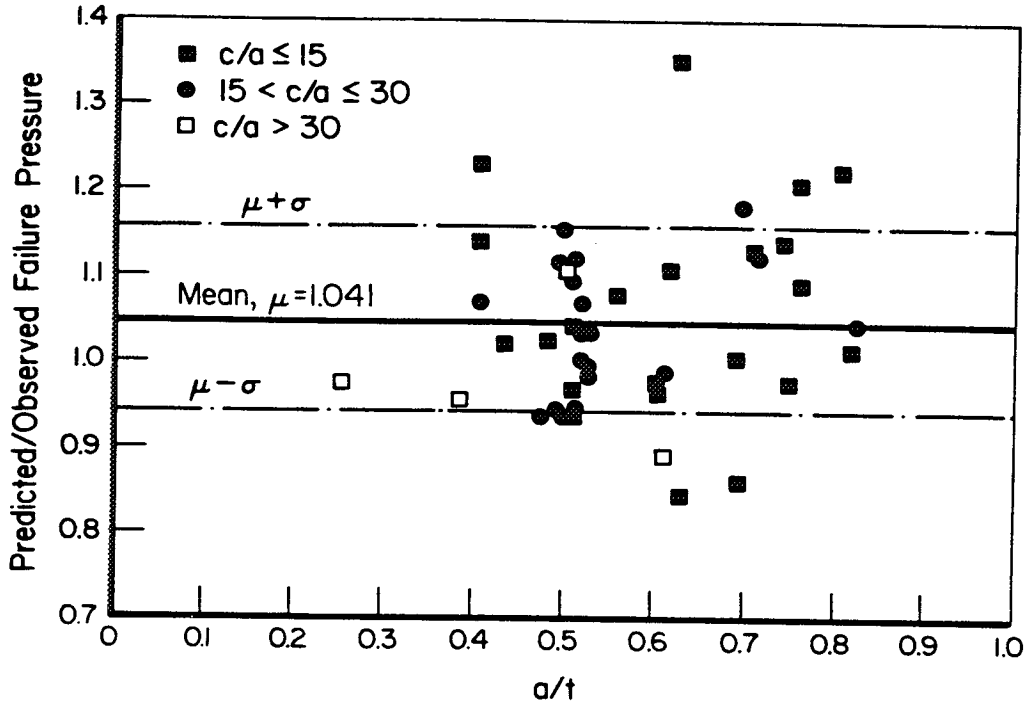

(b) P_p versus a/t and a/c

Figure 5. Comparison of observed and predicted failure pressure for SAPF full-scale tests of PTW flawed line pipe.

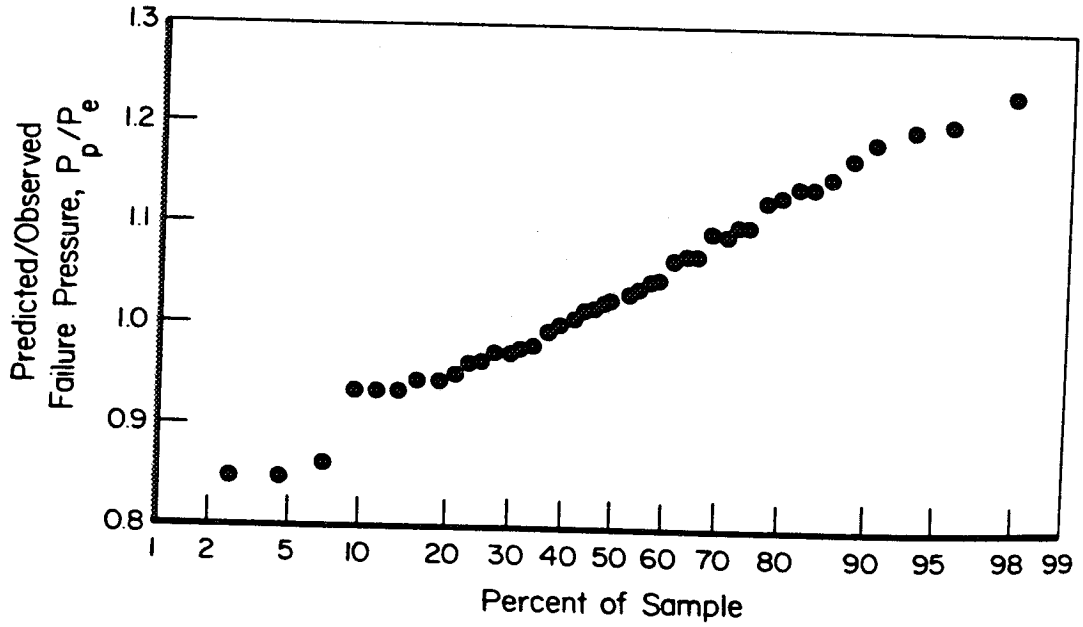

(c) P_p versus Frequency of Occurrence

Figure 5. Concluded.

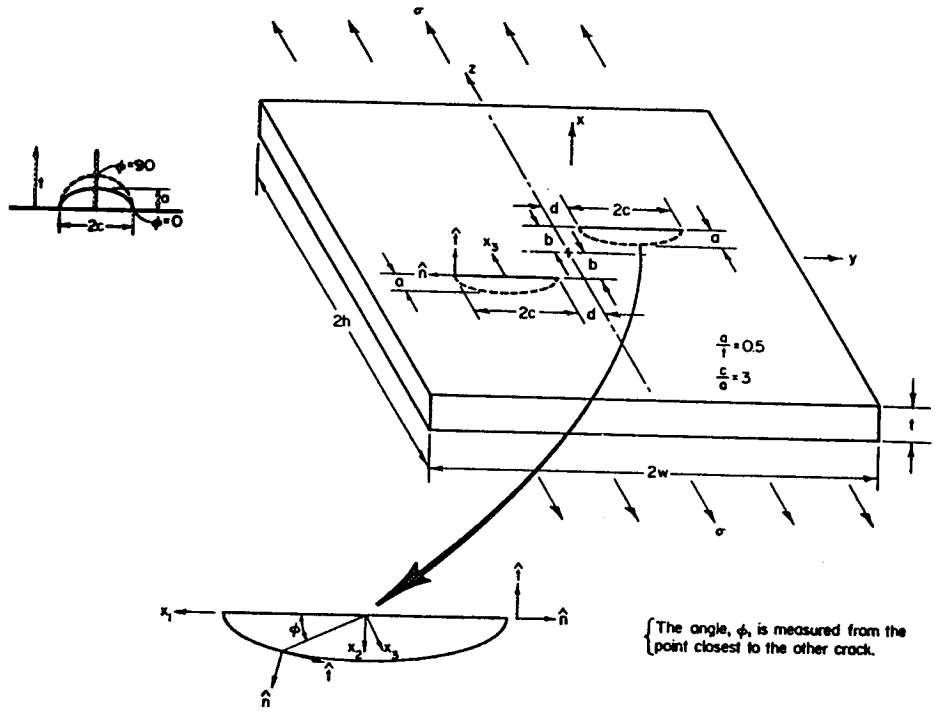

Figure 6. Geometric parameters for a pair of arbitrarily located cracks.

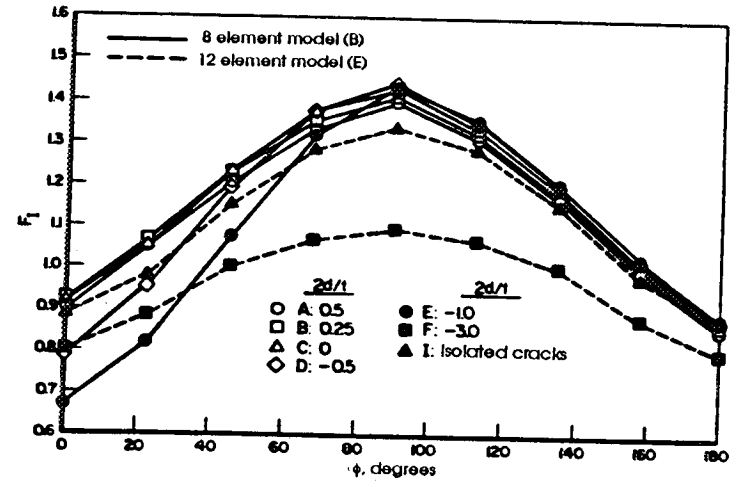

(a) Mode I cracking

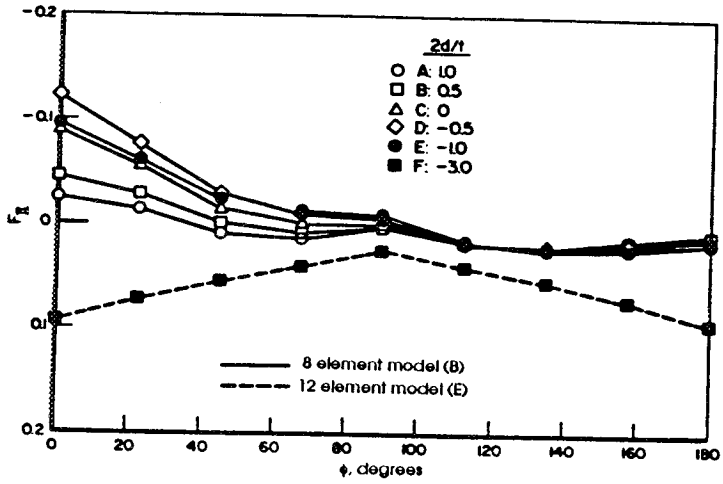

(b) Mode II cracking

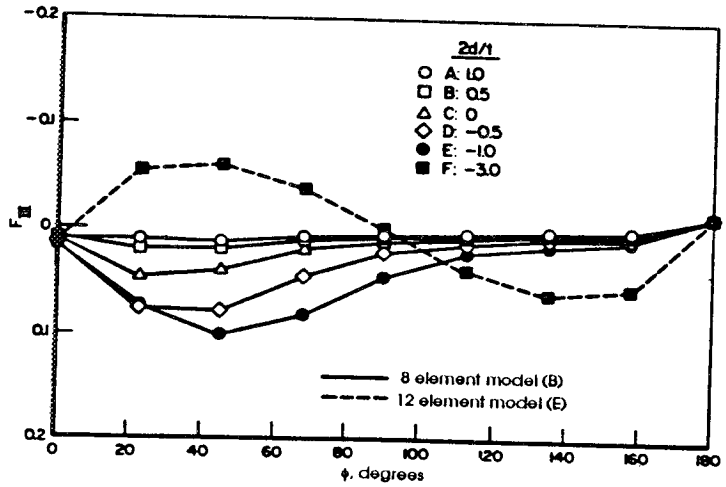

(c) Mode III cracking

Figure 7. Normalized crack driving force as a function of position along the crack front for a pair of cracks for a range of crack positions and depths.